A (GGA+PBE) investigation of MGeBr$_3$ (M = Rb, Cs, Fr) bromide perovskites: structural, electronic, and optical characteristics

O. Alsalmi[a,*], M. M. Saad H.-E.[b]
[a]Physics Department, College of Science, Umm Al-Qura University, P.O. Box 715, Makkah 24382, Saudi Arabia
[b]Department of Physics, College of Science and Arts in Al-Muthnib, Qassim University, Al-Muthnib 51931, Saudi Arabia

First-principles DFT calculations by utilizing FP-LAPW under GGA+PBE method are performed to investigate the structural, electronic and optical characteristics of bromide perovskites MGeBr$_3$ (M = Rb, Cs, Fr). It is found that the cubic structure (Pm-3m) and optimized lattice constants are in good agreement with the previous data. Our GGA+PBE results reveal that MGeBr$_3$ show nonmagnetic semiconductor behavior with direct band-gap (E$_g$ = 0.925 eV (M = Rb), 0.898 eV (M = Cs), 0.952 eV (M = Fr)) along the L–L symmetry direction. Formation energy, octahedral ration and tolerance factor for MGeBr$_3$ have also been calculated. The 2-D charge densities confirm that the chemical bonds (Ge^{2+}–Br$^-$) and (M$^+$–Br$^-$) follow the covalent and ionic bonding types. Moreover, we have calculated and discussed the optical parameters, dielectric constants, absorption, conductivity and refractivity. The calculated electronic and optical properties show the narrow band-gap, high absorption and semiconductor nature making these inorganic materials suitable for optoelectronics applications.

1. Introduction

Various compounds of halide perovskite family have amazing structural, electronic, thermoelectric and optical characteristics that have made them a hot playground for theoretical and experimental research. For example, they are characterized by their: (i) structural and mechanical stability, (ii) chemical stability at high temperatures, (iii) semiconductor electric conductivity, (iv) tunable energy band-gap (E$_g$), (v) charge transport through n-type or p-type, (vi) high ability for optical absorption of light in a wide spectrum range, (vii) wide range of optical emission [1-5]. Moreover, the spectacular thermoelectric properties of such compounds have extensively studied in recent years, due to their suitability for the operation of smart thermoelectric devices [2,3,6]. They fit some applications in this field, such as solar cells, light emitting diodes (LEDs), photovoltaics (PV), and other optoelectronic devices [1-5]. Figure of merit (ZT) ratio is a vital quantity in understanding and evaluating the thermoelectric properties of these compounds. If the ZT value is close to unity (ZT = 1.0), the thermoelectric device works well and gives high thermal efficiency [6-8]. Also, one of the most important conditions that must be met these compounds is the high ratio of power conversion efficiency (PCE), which gives a decisive indicator of the possibility of using them in solar cell potentials. Therefore, scientific research has been heavily pursued on many compounds belong to halide perovskite family to produce reliable, extremely efficient (PCE > 25%), and commercially feasible solar cells [5]. This material science has advanced thanks to recent research studies on the halide perovskites and related compounds for solar cells devices and other optoelectronic applications [1,4]. To increase the PCE of perovskite solar cells, numerous theoretical and experimental research have been done on halide perovskite materials [9-14]. It is worth noting that the negative effect of weather factors on the stability and half-life of solar cells is very important issue and must be taken into account. In-depth studies have

also carried out on additional issues that reduce the commercial expansion of perovskite solar cells, such as low mechanical stability and the toxicity of some element like lead [15-19]. The capability of halide perovskites to absorb light within the UV-VL range should be taken into account when evaluating their applicability in perovskite solar cells technology [1,4,9,11].

Halide perovskites family contains two classes of crystal structures, namely single and double perovskites. Recently, numerous research studies have been done on the cubic perovskite materials, which is the most regular and ideal crystal structure in material science. Based on anion atom X, perovskites are classified into two main types of compounds: (i) perovskite oxides (MBO_3) and (ii) halide perovskites (MBX_3). Halide perovskite MBX_3 materials have found enormous attention in many research fields such as solid state physics, materials science and materials engineering due to their diverse and unique characteristics. Very recently, numerous theoretical and experimental researches have been conducted to study the physical properties of some compounds of metal halide perovskites MBX_3 where (M = alkali metal, B = general metal, and X = halogen element). These MBX_3 perovskites are characterized by a simple chemical composition and their ideal compounds crystallize in a cubic structure with space group of Pm-3m (No. 221). The structure of halide perovskites MBX_3 can be illustrated as M^{1+} and X^{1-} ions shaping a cubic closed-packed (CCP) lattice, where the large B^{2+} ions residing in the octahedral cavities that form by the halogen ions X^{1-} ($M^{1+} X^{1-}_6$). Therefore, the crystal structures consist of 3D net from by the 6-fold corner sharing octahedral MX_6–MX_6 and B^{2+} cations sit in the middle of the 12-fold polyhedral [7,11]. Accordingly, the atomic positions in the unit cell of cubic halide perovskites MBX_3 are: M at (0.0, 0.0, 0.0), B at (0.5, 0.5, 0.5), and X at (0.0, 0.5, 0.5), (0.5, 0.0, 0.5) and (0.5, 0.5, 0.0). Here, the halogen anions are located at the face centered cubic positions, while the M and B cations sit in the corners and middle of the unit cell for MBX_3, respectively. Several metallic M and B atoms can be suitable to yield stable crystal structure of halide perovskites, if they give a tolerance factor (T_F) of about ($T_F = 0.7 – 1.0$) [7,11,20,21].

The primary physical chemical properties of some bromide perovskites $MBBr_3$ have studied by many researchers using different theoretical and experimental techniques. For example, the structural, magnetic, electronic and optical properties of cesium based tin bromide perovskite $CsSnBr_3$ found widely interest in many DFT studies [6,10,11,16,19,20,22,23]. Some authors investigated the main properties of Pb-based compound $CsPbBr_3$ using DFT methods [9,11,24]. Similarly, cesium based germanium bromide perovskite $CsGeBr_3$ have studied by few researchers using the first-principle DFT methods [6,10,11,19,23]. While, bromide perovskites $MBBr_3$ compounds with (M = Na, K, Rb, Fr; B = Ge, Sn) found less attention [14,18,23]. In the present study, we have investigated the crystal structure, optical and electronic properties of three alkali metal compounds of bromide perovskites $MGeBr_3$ (M = Rb, Cs, Fr) by using the FP-LAPW method. The motivation of this study is to improve the FP-LAPW calculations and to provide some additional information to the characteristics of $MGeBr_3$ perovskites using the (GGA+PBE) approximation. The current FP-LAPW calculations were carried out by utilizing the PBE functional based on the generalized gradient approximation (GGA), to well describe the physical chemical properties of $MGeBr_3$ compounds. This study provides a notable contribution in halide perovskites field. Here, we show that the type of M site affects the structural, optical and electronic properties of germanium bromide perovskite $MGeBr_3$. Also, we investigate the structural stability of these crystals and the results confirm that $MGeBr_3$ perovskites show a stable structure. Findings show that these materials exhibit unique physical characteristics such as structural stability, semiconductors nature, high optical absorption and other features. These properties make bromide perovskites $MGeBr_3$ (M = Rb, Cs, Fr) suitable inorganic materials for a variety of modern applications like photovoltaics solar-cells, photosensors, photodiodes, photodetectors, and other optoelectronics devices.

2. Computational methodology

The structural, electronic and optical characteristics of bromide perovskites $MGeBr_3$ (M = Rb, Cs, Fr) are calculated using the first-principles density functional theory (DFT) [25], as implemented in the WIEN2k code [26]. The useful method of full potential (FP) linearized

augmented plane wave (LAPW) is exploited in these calculations. We applied the Perdew-Burke-Ernzerhof (PBE) functional [27], in the frame of Generalized Gradient Approximation (GGA) [28] to evaluate the structural and optoelectronic properties of these materials. Non spin-polarized version of the PBE+GGA calculations is performed to obtain the appropriate results of the physical chemical properties of $MGeBr_3$ compounds. In PF-LAPW scheme, the unit cell of three perovskites $MGeBr_3$ encloses two chief regions; (i) the first of which is a spherical region, muffin-tin (MT), and it is definite by ($r \leq R_{MT}$) where R_{MT} is the muffin-tin radius. The potential in MT region is expected to be spherically symmetric. In all GGA+PBE calculations, the values of R_{MT} for the individual atoms in ($M^+Ge^{2+}Br_3^-$) crystals are set as [R_{MT} (M^+) = 2.2 a.u., R_{MT} (Ge^{2+}) = 2.0 a.u., and R_{MT} (Br^-) = 1.8 a.u.]. In atomic MT region, the solution of Schrödinger equation is given by the radial function times a spherical harmonic, while in the interstitial region (IR), the potential is considered to be constant and the Schrödinger equation is solved by plane wave (PW) functions.

The ground state energy convergence to (0.0001 Ry) was achieved using the total number of (k-points = 2000) in the first Brillouin zone (BZ) with a cutoff value ($R_{MT}K_{max}$ = 7.0), where R_{MT} corresponds to smallest MT radius and K_{max} is the largest reciprocal lattice vector [11,15]. We set the electronic configurations of the individual atoms M (M = Rb, Cs, Fr), Ge, and Br in their bromide perovskite $MGeBr_3$ as follow: Rb [Kr] $5s^1$, Cs [Xe] $6s^1$, Fr [Rn] $7s^1$, Ge [Ar] $4s^2$ $3d^{10}$ $4p^2$, and Br [Ar] $4s^2$ $3d^{10}$ $4p^5$, respectively. The structural optimizations of $MGeBr_3$ were carried out as a first stage, where the unit cell energy has been varied with respect to its unit cell volume.

3. Results and discussion

In this section, we show the calculations results and discussion of main physical and chemical properties of the investigated materials in present study.

3.1. Structural properties
3.1.1. Structural parameters
The family of Ge-based bromide perovskites $MGeBr_3$ (M = Rb, Cs, Fr) belong to the cubic structure symmetry having space group of Pm-3m number 221. As shown in Fig. 1, the unit cell of these crystal structures consists of five atoms with formula unit (Z = 1). In this unit cell of cubic $MGeBr_3$, one type of alkali atom M = Rb, Cs, Fr occupies 1a (0, 0, 0) positions, the second Ge atoms sits at 1b (½,½,½), and halogen atoms Br sit at 3c positions with (0, ½, ½), (½,0, ½) and (½, ½, 0). Table 1 shows the data that used in the WIEN2k.

Table 1. The atomic sites, Wyckoff positions, and coordinates (x, y, z) in the cubic unit cell (Pm-3m; Z = 2), shown in Fig. 1, of perovskites $MGeBr_3$ (M^{1+} = Rb, Cs, Fr).

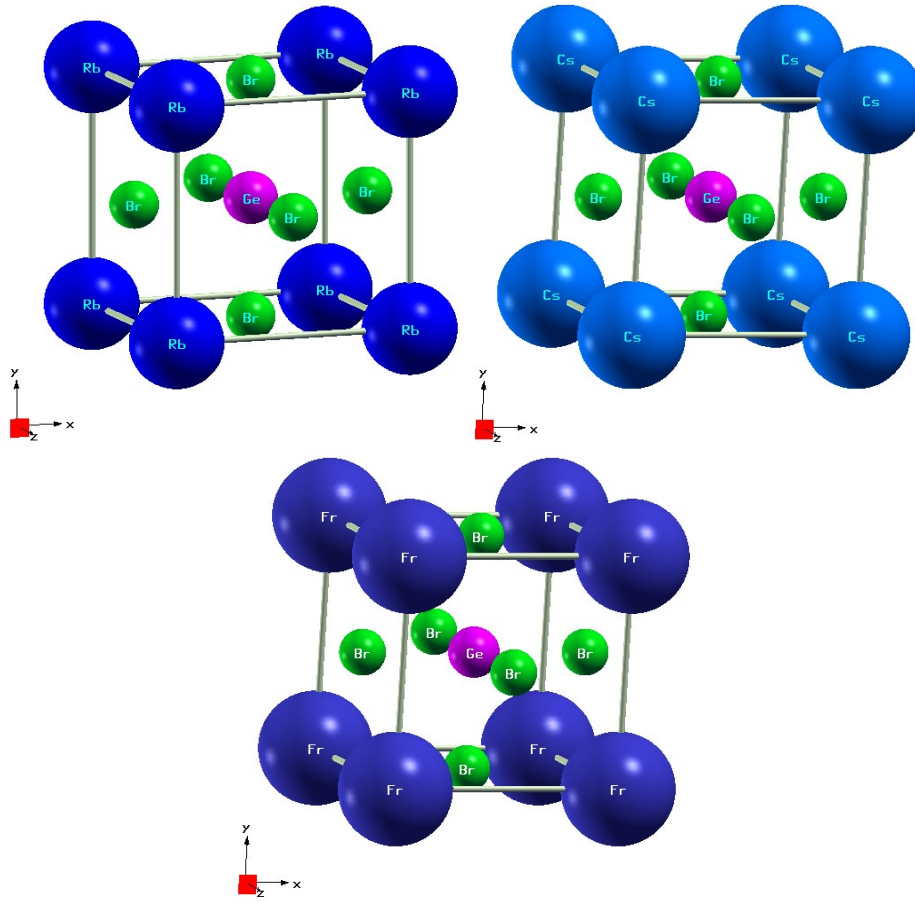| Site	Radius (Å)	Wyckoff position	Site symmetry	Atomic coordinates		
				x	y	z
M^+-cation	Rb(1.87); Cs(1.92); Fr(1.94)	1a	m-3m	0	0	0
Ge^{2+}-cation	0.87	1b	m-3m	½	½	½
Br^--anion	1.82	3c	4/mm.m	0	½	½
				½	0	½
				½	½	0

Fig. 1. Crystal structure of RbGeBr₃, CsGeBr₃ and FrGeBr₃.

The study and finding the equilibrium state are carried out by tracing the variation of the total energy according to change in the volume of the unit cell. To begin with the detailed investigation of the main physical properties of perovskites $MGeBr_3$ (M = Rb, Cs, Fr), we first performed calculations of the structural optimization for these systems using GGA+PBE functional. Fig. 2 plots the variation of total energy as a function of the volume per unit cell of bromide perovskites $RbGeBr_3$, $CsGeBr_3$ and $FrGeBr_3$. Then, we fitted the optimization of total energy versus volume by the Murnaghan equation of state [29].

$$E = E_0 + \frac{B}{B_P}(V - V_0) + \frac{B}{B_P(B_P - 1)}\left[V\left(\frac{V_0}{V}\right)^{B_P} - V_0\right] \tag{1}$$
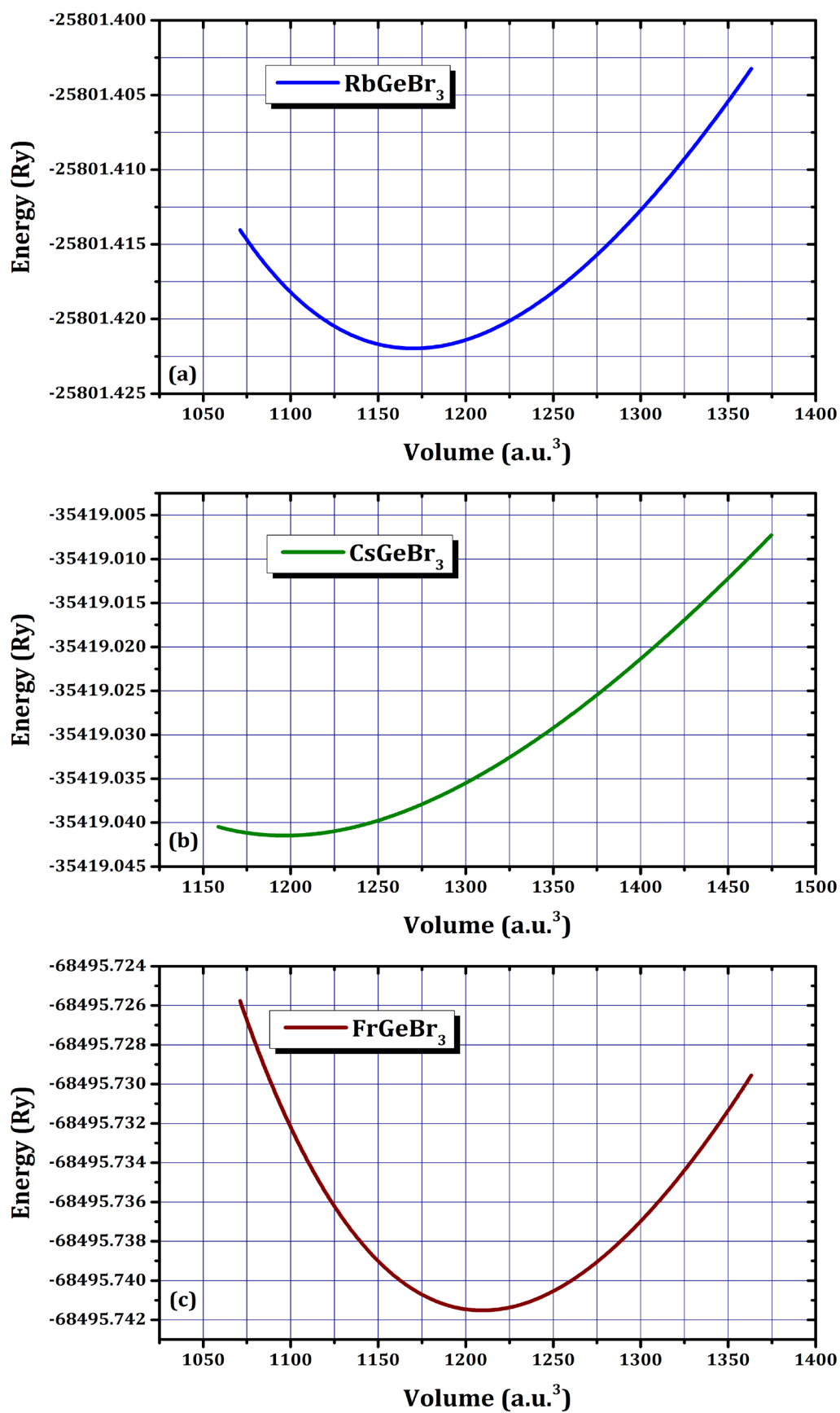
Fig. 2. Calculated total energy as a function of volume for RbGeBr$_3$, CsGeBr$_3$ and FrGeBr$_3$.

From the curves in Fig. 2(a,b,c), we find the minimum energy, i.e. the ground state energy (E_0) of MGeBr$_3$ perovskites which corresponds to the optimum volume, i.e. the equilibrium volume (V_0). Table 2 reports the values of these V_0 and E_0 plus optimized structural parameters, lattice constants (a_0), bulk modulus (B) and its pressure derivatives (B_P). The obtained parameters indicate that all MGeBr$_3$ compounds show minimum energy in the cubic crystal structure.

Table 2. The structural parameters of optimized unit cell for MGeBr$_3$ (M^{1+} = Rb, Cs, Fr).

MGeBr$_3$	a_0 (Å)	V_0 (Å^3)	B (GPa)	B_P (GPa)	E_0 (Ry)
RbGeBr$_3$	5.5762 5.853[a] 5.530[b]	173.38	23.496	5.0000	-25801.422
CsGeBr$_3$	5.6205 5.636[c] 5.587[d]	177.55	24.015	5.0000	-35419.042
FrGeBr$_3$	5.6383 5.630[e]	179.24 178.42[d]	22.898	5.0000	-68495.742

[a] Ref. (30); [b] Ref. (31); [c] Ref. (32); [d] Ref. (33); [e] Ref. (14)

Table 3 summarizes the optimized atomic distances in the unit cell of three compounds of cubic bromide perovskites MGeBr$_3$ (M = Rb, Cs, Fr). It can see that the calculated lattice constants and bond distances of FrGeBr$_3$ are greater than those for the other two perovskites, which is mainly due to the radius effect of the alkali atom M = Rb, Cs, Fr. Also, the current results are in good agreement with available data of similar halide perovskites [11,14,19,23].

Table 3. The optimized atomic distances in the unit cell of MGeBr$_3$ (M^{1+} = Rb, Cs, Fr).

MGeBr$_3$	M$^+$–M$^+$ (Å)	M$^+$–Ge^{2+} (Å)	M$^+$–Br$^-$ (Å)	Br$^-$–Br$^-$ (Å)	Ge^{2+}–Br$^-$ (Å)
RbGeBr$_3$	5.5762	4.8291	3.9430	5.5762	2.7881
CsGeBr$_3$	5.6205	4.8675	3.9743	5.6205	2.8102
FrGeBr$_3$	5.6383	4.8829	3.9869	5.6383	2.8191

3.1.2. Structural stability

Ge-based bromide perovskites MGeBr$_3$ own two essential features that decide its suitability in solar cells applications, i.e. stability and efficiency. To examine the structural stability and lattice distortion of studied perovskites MGeBr$_3$, one can compute the values of octahedral ($\mathcal{F}$) and tolerance (τ) factors. Therefore, these two structural factors are very important empirical parameters allow evaluating the structure stability and predicting new perovskite compounds.

Octahedral factor $\mathcal{F}$, which is a crucial stability factor evaluates the fitting of Ge^{2+} cations into their octahedra network [Ge^{2+}Br$_6$], can be estimated by the cation-anion ratio [34,35]:

$$\mathcal{F} = \frac{R_{Ge}}{R_{Br}} \tag{2}$$

By using the ionic radii of Ge^{2+} and Br$^-$ in the VI-coordinate arrangement, (R$_{Ge}$ = 0.870 Å) and (R$_{Br}$ = 1.820 Å) [36], the calculated value of octahedral factor is ($\mathcal{F}$ = 0.478). This result belongs to the range ($\mathcal{F}$ = 0.440–0.900) [34,35], which confirms the stable of crystal structure for all perovskites with MGeBr$_3$ system.

The values of tolerance τ for the Ge-based bromide perovskites MGeBr$_3$ are determined by using the ionic ratio of their major bond distances (M$^+$–Br$^-$) and (Ge^{2+}–Br$^-$), as follow [37]:

$$\tau = 0.707 \frac{[R_M + R_{Br}]}{[R_{Ge} + R_{Br}]} \tag{3}$$

Here, we set the ionic radii of M atoms (R_{Rb} = 1.870 Å, R_{Cs} = 1.920 Å, R_{Fr} = 1.940 Å) from XII-coordinate arrangement, and (R_{Ge} = 0.870 Å) and (R_{Br} = 1.820 Å) in the VI-coordinate arrangement [36]. We found that the tolerance factor of our perovskites MGeBr$_3$ is (τ = 0.970; M = Rb), (τ = 0.983; M = Cs) and (τ = 0.988; M = Fr). The obtained results match with the cubic structure symmetry (Pm-3m) of MGeBr$_3$ compounds [11,20,33]. Also, they very close to ideal tolerance factor (τ = 1.0) indicating no structural distortion in the studied crystal structure.

To determine the thermodynamic stability of cubic bromide perovskites MGeBr$_3$ (M = Rb, Cs, Fr), we have calculated their formation energy (ΔF_E). It represents the difference energy between the total energy per unit cell of MGeBr$_3$ and the sum of energies per atom:

$$\Delta F_E = E_{MGeBr_3} - [E_M + E_{Ge} + 3E_{Br}] \tag{4}$$

At equilibrium state, the formation energy per unit cell of MGeBr$_3$ structures is found to be ΔF_E = -0.56 to -0.84 Ry (-7.62 to -11.43 eV). The negative and small ΔF_E shows that MGeBr$_3$ is chemically stable and can be synthesis in laboratory by using experimental methods [11].

3.2. Electronic properties
3.2.1. Band structures

Fig. 3(a,b,c) shows the behavior of band structures of studied bromide perovskites MGeBr$_3$ (M = Rb, Cs, Fr), involving the GGA+PBE approximation for nonmagnetic state. The band structures are calculated along the high cubic symmetry directions within the first Brillouin zone (BZ). It can be seen that the maximum of the valence bands (VB) concurs with the minimum of the conduction bands (CB) all along the L–L symmetry direction, which exposes the semiconductive feature of these compounds. The calculated values of direct band gap (E_g) using GGA+PBE method for three perovskites are listed in Table 4. The obtained results of band structures in Fig. 3(a,b,c) reveal that the M = Fr based perovskite shows wider band gap E_g than that show by M = Rb and M = Cs systems. Our calculated results of the band gap for the semiconductors MGeBr$_3$ are slightly higher than the previous DFT data for related halide perovskites [30-33,38].
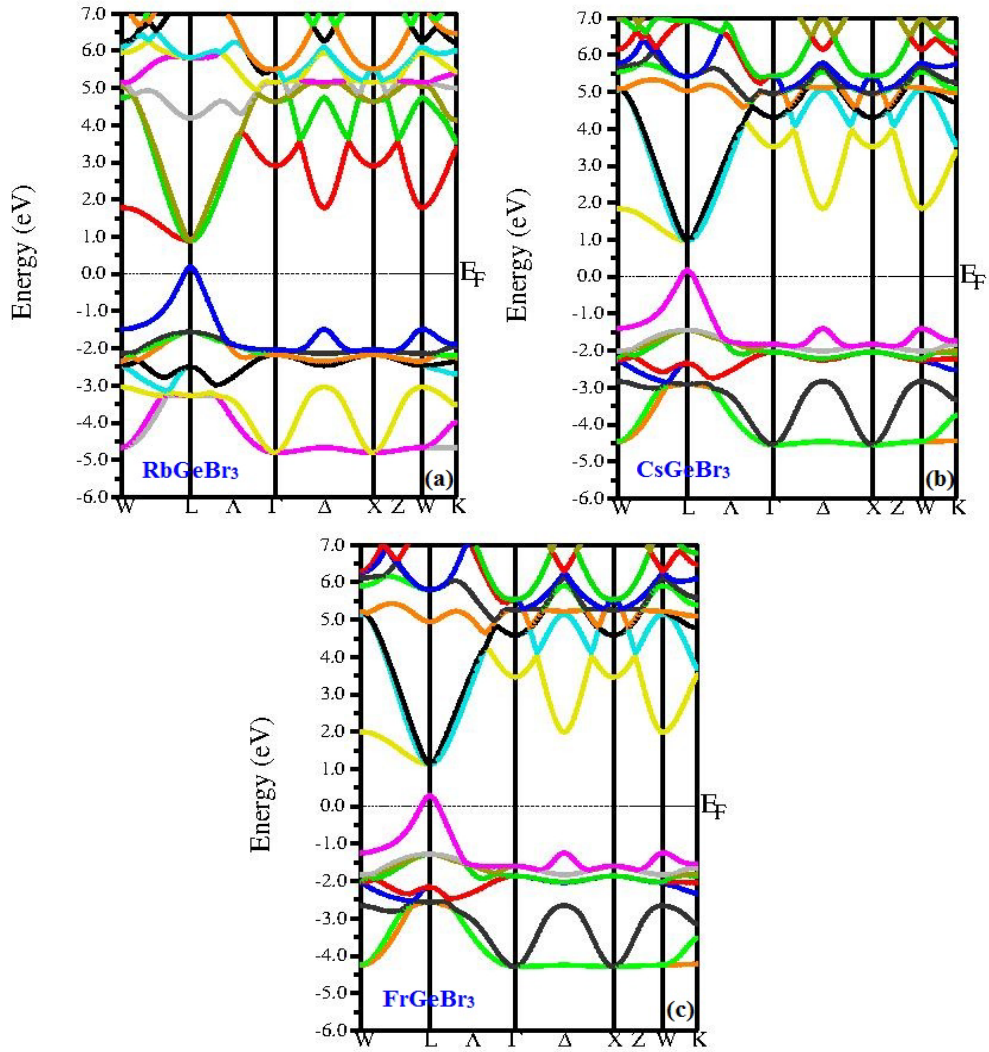
Fig. 3. Calculated band structures for RbGeBr₃, CsGeBr₃ and FrGeBr₃.

Table 4. The energy band gap of MGeBr₃ (M^{1+} = Rb, Cs, Fr).

MGeBr₃	E_g (eV)	VBM (eV)	CBM (eV)
RbGeBr₃	0.925 0.980[a] 1.100[b]	-0.026	0.899
CsGeBr₃	0.898 1.490[c] 0.707[d]	-0.017	0.881
FrGeBr₃	0.952 0.810[e]	-0.021	0.931

[a] Ref. (30); [b] Ref. (32); [c] Ref. (33); [d] Ref. (38); [e] Ref. (14)

3.2.2. Density of states

Further, the total density of states (TDOS) and partial density of states (PDOS) of these perovskite compounds calculated by the GGA+PBE approximation are shown in Figs. 4, 5 and 6, respectively. In all figures, we plot the behavior of TDOS for the unit cells of MGeBr₃ and their atoms M, Ge and Br (panels (a)).
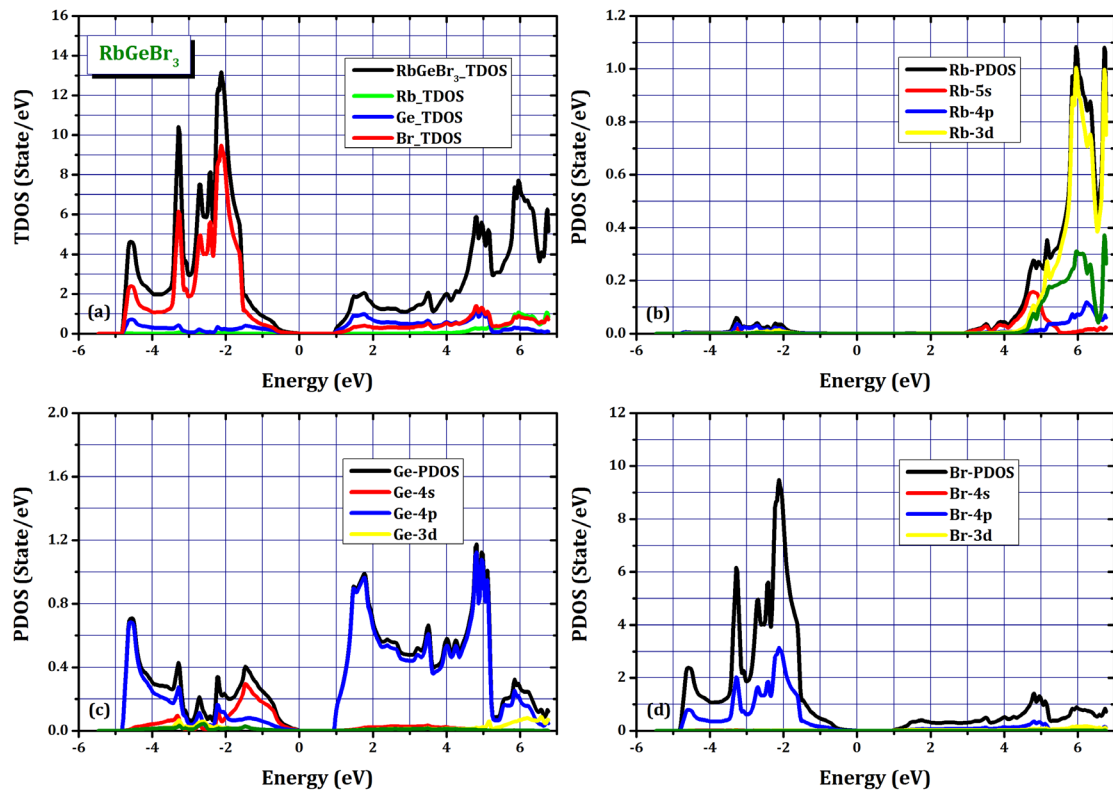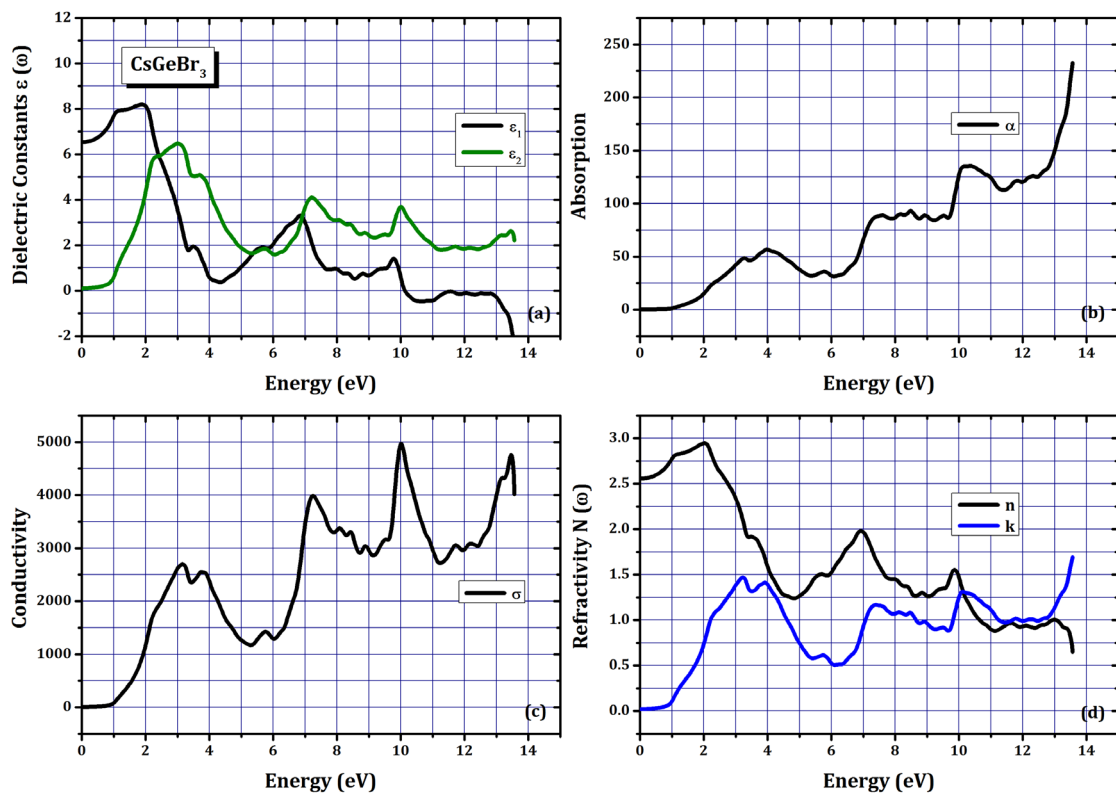
Fig. 4. Calculated TDOSs and PDOSs for RbGeBr₃.
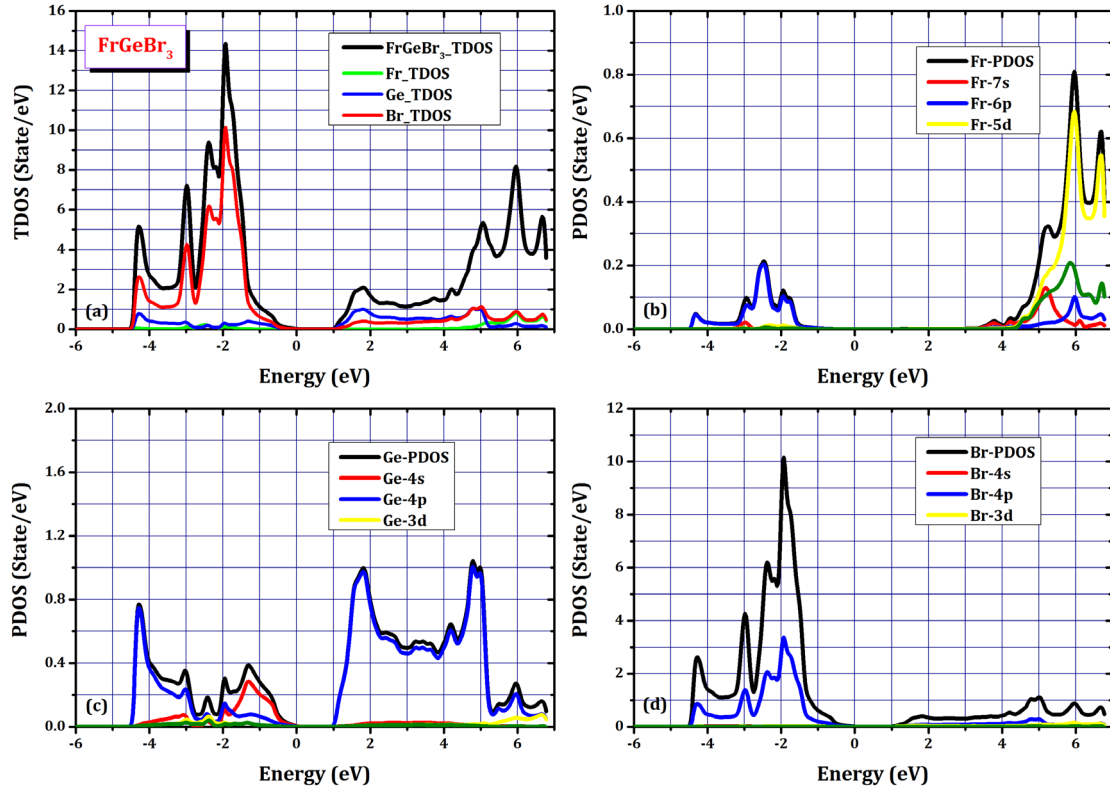

Fig. 5. Calculated TDOSs and PDOSs for CsGeBr₃.

Fig. 6. Calculated TDOSs and PDOSs for FrGeBr₃.

Besides, the projected PDOSs of s, p, and d orbitals are calculated and illustrated in (panels (b, c, d)) along with these TDOSs. We can clearly see that all TDOSs of $MGeBr_3$ also show band gap (E_g) near the Fermi level, 0.0 eV, which confirms the semiconductor nature of these perovskites. And this is also strong evidence that proves our calculations of the band structures, Fig. 3. The VB of $MGeBr_3$ structures is mainly dominated by the halogen Br-4p orbital plus a small effect comes from metalloid Ge-4s and Ge-4p orbitals. Whereas, the CB is mainly dominates by the hybridization of metalloid and halogen orbitals through the partial Ge-4p and Br-4p states. The partial states of alkali atom in M-s, M-p and M-d orbitals appear far away from the Fermi level in the CB region.

3.2.3. Charge density

In order to take a deep insight and explore the nature of electronic structures of M–Ge–Br systems, we calculated the 2-D charge density in the (100) plane. Fig. 7 presents the 2-D charge density of the unit cell for the three compounds of bromide perovskites $MGeBr_3$ (M = Rb, Cs, Fr) using the contour style. These 2D charge density plots allow visualizing the behavior of the chemical bonds between the compound atoms in its unit cell. Also, they elucidate the mechanism of charge carries transport through these bonds in $MGeBr_3$ crystals. We can see from the 2-D charge density plots of $MGeBr_3$, and their partial densities of states PDOSs that shown in Figs. 4-6, there is hybridization between the 4p orbital of cation (Ge^{2+}-4p) and anion (Br^--4p).

The hybridization arrangement of these orbitals indicates that the type of chemical bonding between the cation Ge^{2+} and anion Br^- (Ge^{2+}– Br^-) prefers the covalent bond nature. This observation can be inferred by the dense number of contour lines around each of the cation Ge^{2+} and anion Br^-. The center of this covalent bond is in the middle of unit cell of cubic $MGeBr_3$, where the cation Ge^{2+} sits in 1b (½,½,½) site and six anions Br^- occupy the 3c site with three positions (0, ½, ½), (½,0, ½) and (½, ½, 0).

Also, there is a second type of chemical bond in MGeBr$_3$ crystals; i.e. the ionic bonds between metallic cations M$^+$ (M = Rb, Cs, Fr), which occupy the corners sites, and the halide anions Br$^-$. Thus, the (M$^+$– Br$^-$) bonds which show ionic nature emerge as sparse with low density and semi-isolated contour lines surrounding M$^+$ and Br$^-$. Accordingly, it is clear from all 2-D charge density plots, the three ions M$^+$, Ge^{2+} and Br$^-$ in bromide perovskite compounds MGeBr$_3$ show a covalent-ionic mixture in their internal chemical bonding.
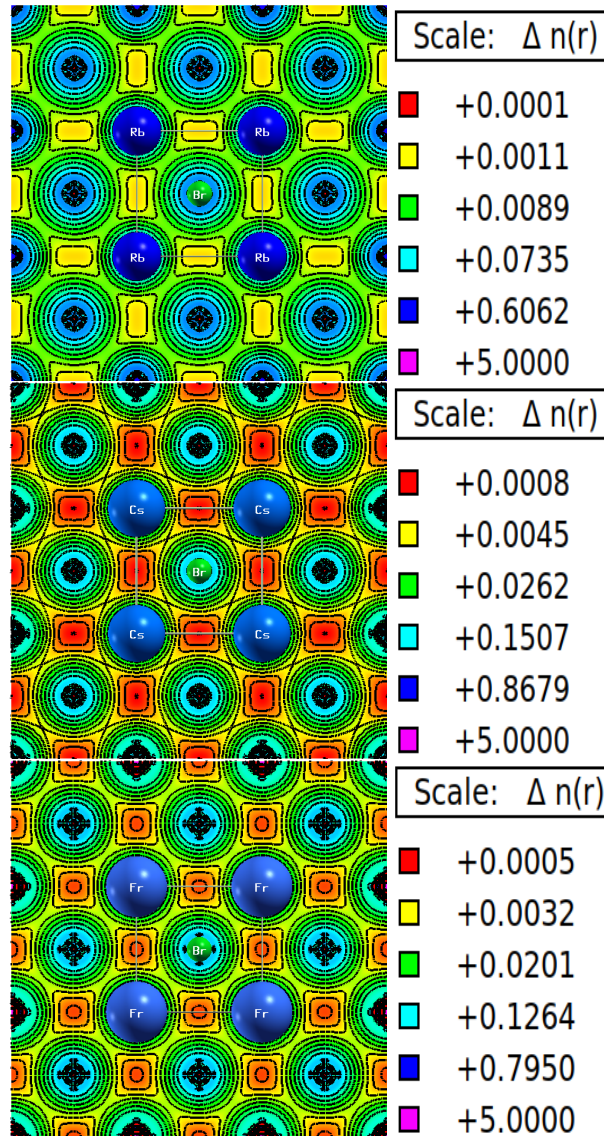

Fig. 7. Calculated charge density for RbGeBr$_3$, CsGeBr$_3$ and FrGeBr$_3$.

3.3. Optical properties

The possibility of utilizing semiconductor materials in various optoelectronic applications due to their exciting properties, we investigated the optical parameters of bromide perovskites MGeBr$_3$ (M = Rb, Cs, Fr). So, the frequency-dependent (ω) optical parameters of these materials were calculated by means of behavior of their optical dielectric function $\varepsilon(\omega)$. This $\varepsilon(\omega)$ portrays the optical properties of MGeBr$_3$ structure via a complex function contains two terms, imaginary $\varepsilon_2(\omega)$ and real $\varepsilon_1(\omega)$; i.e. $\varepsilon(\omega) = i\varepsilon_2(\omega) + \varepsilon_1(\omega)$. Optical parameters of MGeBr$_3$ (M = Rb, Cs, Fr), dielectric constants ε, absorption α, conductivity σ, refractivity N, are calculated and shown in Figs. 7, 8 and 9, respectively.
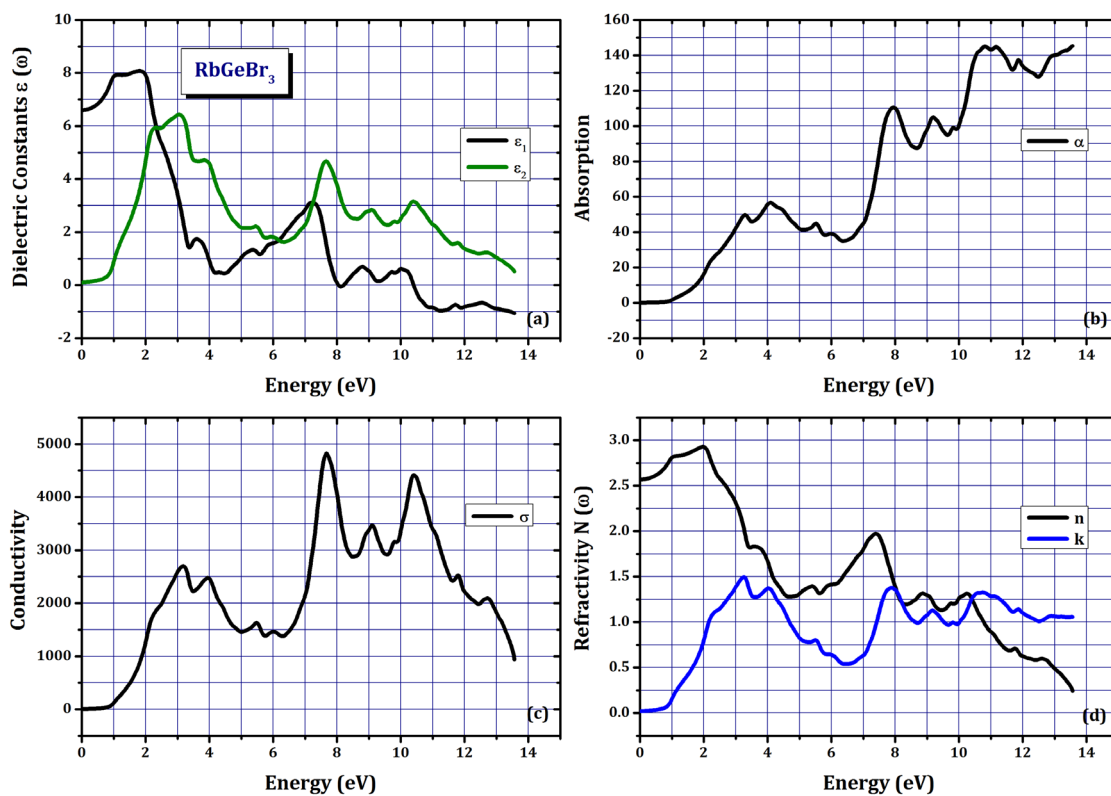
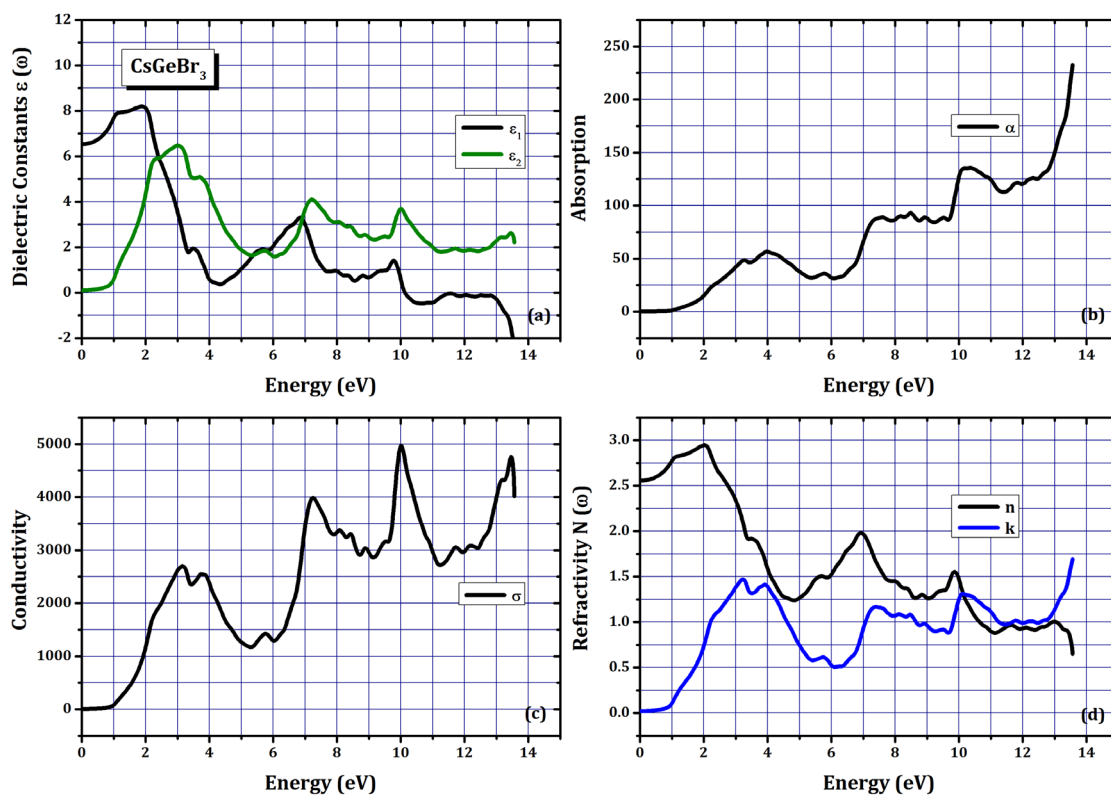*Fig. 8. Calculated optical parameters for RbGeBr₃.*

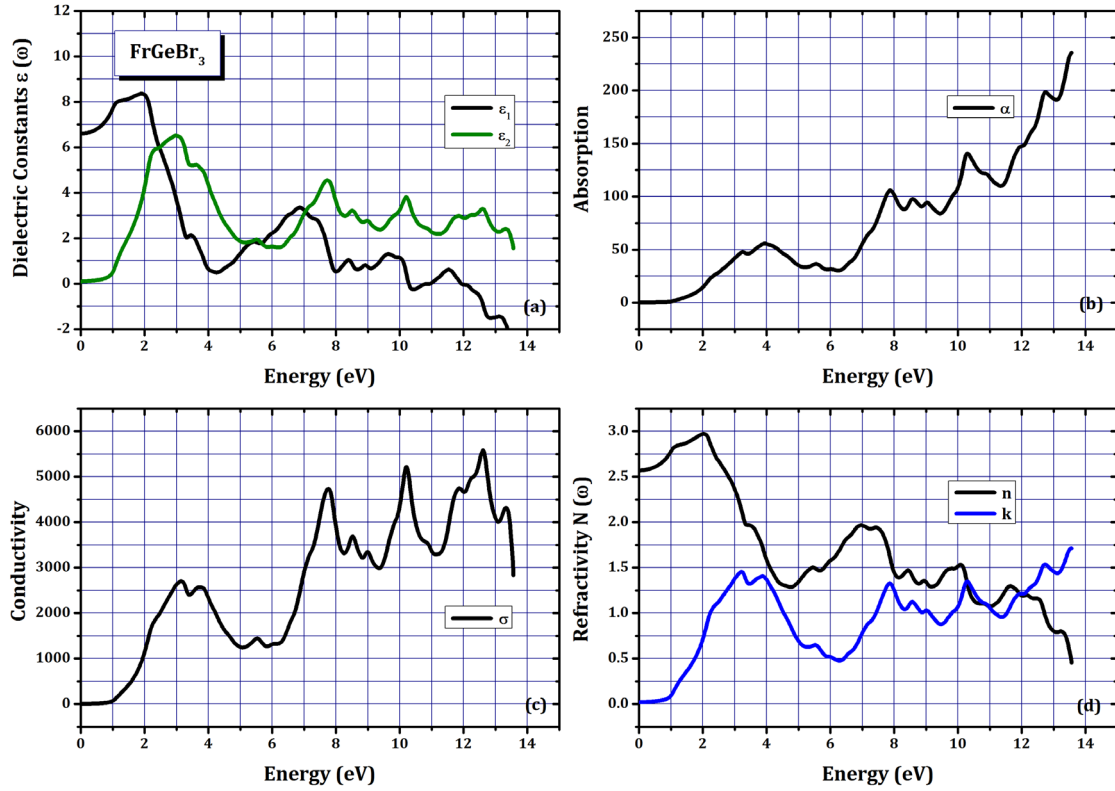*Fig. 9. Calculated optical parameters for CsGeBr₃.*

Fig. 10. Calculated optical parameters for FrGeBr₃.

3.3.1. Dielectric constants

First, the behavior of dielectric constants is described by the results of real ε_1 and imaginary ε_2 terms and illustrated in Figs. 7(a), 8(a) and 9(a). The real dielectric constant ε_1 exhibits the polarization level on the material of MGeBr₃ crystals. We can see that the start point of real dielectric constant ε_1 gives the static value $\varepsilon_{1(0)}$ of about 6.60, 6.53 and 6.60 for MGeBr₃ (M = Rb, Cs, Fr), respectively. Next, the value of ε_1 increases as the photon energy increases to its highest peak $\varepsilon_{1(m)}$, of about 8.06, 8.19 and 8.36, , respectively, at a similar point with an energy of 1.89 eV. Beyond the point with 2.0 eV, the ε_1 spectra decrease sharply with few value fluctuations until they reach higher energy of 8.0 eV and become flat with ε_1 value of about unity. This characteristic reveals the transparent behavior of MGeBr₃ perovskites at high energy [39-41]. We can also see that the spectra of ε_1 show negative values at an energy more than 10 eV. Which imply that the incident photons are attenuated in these materials indicating that MGeBr₃ behave as optical conductors in the higher energy values. Second, from the plots of imaginary part ε_2 in Figs. 7(a), 8(a) and 9(a), which illustrate the total absorption of light by the studied materials, we can see all spectra of MGeBr₃ perovskites show similar dielectric behavior. The ε_2 spectra have three critical values of about 6.48, 4.45 and 3.55 at similar energy points 3.0, 7.50 and 10.2 eV, respectively.

3.3.2. Absorption

The behavior of optical absorption α for the three compounds of MGeBr₃ perovskites is shown in Figs. 7(b), 8(b) and 9(b), respectively. This parameter depends mainly on the values of real ε_1 and imaginary ε_2 parts as well as the photons energy ω of light. Since there is interaction between the energetic electrons in MGeBr₃ structure and the absorbed photons of incident light [20], we can use these α spectra evaluate the optical response of MGeBr₃ materials. At zero energy, the α spectra of MGeBr₃ reveal that the optical gap values are 1.0, 0.90 and 0.97 eV, respectively. The results of optical gap closely relate to those obtained from DOSs and band

structures, Table 4, indicating similar structures of energy band contribution in the optoelectronic transitions from valence to conduction bands. The calculated results in all three figures confirm that the α spectra increase with the absorbed energy. We can see that MGeBr$_3$ compounds show high absorption α fits the visible light to ultraviolet (VL-UV) range, which shows the superior potential of perovskites MGeBr$_3$ for optoelectronics devices that operate in this range [39].

3.3.3. Conductivity

In Figs. 7(c), 8(c) and 9(c) we show the results of calculated optical conductivity σ for the studied bromide perovskites MGeBr$_3$, which depends on photons energy and ε_2 part. It clarifies the optoelectronic conduction due to the incident photons on the crystal structure of MGeBr$_3$ [39,40]. All σ spectra start from the zero value at zero energy and then increase to show an obvious peak at high energies range. The start points of σ spectra have energy of about 1.10, 0.95 and 0.98 eV, which are very close to those band gaps found in band structures and DOSs, Figs. 3-6. Also, the maximum values of σ are that for MGeBr$_3$, 4816.77 at 7.66 eV (M = Rb), compared to another perovskites (M = Cs) and (M = Fr) which they equal to 4964.66 and 5583.54 at the high energy points of 10.0 eV and 12.6 eV, respectively. Moreover, we can view from the σ spectra that the gradually raise of conductivity occurs in the VL-UV region. Here, the change of M site in MGeBr$_3$ (M = Rb, Cs, Fr) causes an increase in the optical conductivity σ and the (M = Fr) state shows the highest conductivity.

3.3.4. Refraction

As shown in Figs. 7(d), 8(d) and 9(d), the optical refraction $N(\omega)$ of bromide perovskites MGeBr$_3$ contains only two indexes $N(\omega) = n(\omega) + ik(\omega)$. The real part is called refractivity n and the imaginary part refers to extinctivity k which are determined using the values of real ε_1 and imaginary ε_2 dielectric constants [20]. Similar to that notice in conductivity and absorption, the n spectra start from a static refractivity n_0 of about 2.56 for these three compounds and decrease past this point. Then their n index increases to reach its maximum refractivity of 2.93, 2.95 and 2.97, respectively, at similarly energy point of about 2.0 eV that fits in the visual field of VL range. Finally, the n spectra decrease at high energies more than 7.5 eV beyond maximum peaks, and at some energy points, it shows values less than unity. Thus, the MGeBr$_3$ materials show superluminal nature within this energy range [42]. The extinctivity k is a vital criterion that allows determining the optical fluorescence; large k confirms that MGeBr$_3$ have high optical fluorescence nature and their absorption increases [39]. From the plots in Figs. 7(d), 8(d) and 9(d), it can be observed that the behavior of all k spectra closely follow their corresponding ε_2 spectra. Besides, the k spectra contain two maximum peaks of about 1.50 and 1.30 appear in two energy ranges, 2.0 to 3.25 eV and 7.0 to 8.0 eV, which match the VL and UV ranges, respectively. The calculated results of optical parameters for MGeBr$_3$ are in good agreement with those obtained for similar halide perovskites AGeBr$_3$ with (A = Fr, Rb, Cs) [6,11,14,23,31].

4. Conclusions

In this paper, we carried out first-principles calculations in the frame of density functional theory (DFT) to investigate the structural, electronic and optical characteristics of three compounds of Ge-based bromide perovskites MGeBr$_3$ (M = Rb, Cs, Fr). According to full-potential linearized augmented plane wave (FP-LAPW) method, the DFT calculations have been performed by using the generalized gradient approximation (GGA+PBE) in the Wien2k program.

The structural optimization confirms the cubic structure (Pm-3m space group) of MGeBr$_3$ compounds with lattice constant of (a_0 = 5.5762 Å; M = Rb), (a_0 = 5.6205 Å; M = Cs) and (a_0 = 5.6383 Å; M = Fr). All systems of Ge-based inorganic bromide perovskites MGeBr$_3$ give band structures and densities of states DOSs which reveal their nonmagnetic (NM) and semiconductor characteristics. MGeBr$_3$ show proper values of the direct band-gap along the L-L symmetry directions of (E$_g$ = 0.925 eV; M = Rb), (E$_g$ = 0.898 eV; M = Cs) and (E$_g$ = 0.952 eV; M = Fr). Based on the results of 2-D electronic charge density, the chemical crystal structure of bromide

perovskites $MGeBr_3$ incorporates mixture of covalent (Ge^{2+}–Br^-) and ionic (M^+–Br^-) bonding, which satisfies the essential conditions of structural stability for the (Pm-3m) crystals.

Furthermore, we calculated and discussed the optical characteristics that include the dielectric function ε parts, real ε_1 and imaginary ε_2, conductivity σ, absorption α, refractivity n and extinctivity k. According to the results of these optical parameters, the crystal structure of all bromide perovskites $MGeBr_3$ shows a wide range of optical absorption α with a high optical refractivity n close to the visible and ultraviolet ranges. The obtained characteristics in this study, such as structural stability, direct band-gap, and high absorption and refraction, candidate these $MGeBr_3$ materials to be used as optical harvesters in photovoltaic solar cells and other optoelectronics devices.

References

[1] T. Leijtens, K. A. Bush, R. Prasanna, M. D. McGehee, Nature Energy **3**, 828 (2018); https://doi.org/10.1038/s41560-018-0190-4

[2] R. Sharma, A. Dey, S. A. Dar, V. Srivastava, Comput. Theor. Chem. **1204,** 113415 (2021)**;** https://doi.org/10.1016/j.comptc.2021.113415

[3] S. Khan, A. Gassoumi, A. U. Rahman, F. Ullah, R. Ahmad, N. Mehmood, M. Abdul, and A. H. Shah, Phys. Scr. **98**, 055907 (2023); https://doi.org/10.1088/1402-4896/acc6fa

[4] M. Manzoor, M. W. Iqbal, M. Imran, N. A. Noor, A. Mahmood, Y. M. Alanazi, S. Aftab, J. Mater. Res. Technology **18**, 4775 (2022); https://doi.org/10.1016/j.jmrt.2022.04.073

[5] J. Yuan, A. Hazarika, Q. Zhao, X. Ling, T. Moot, W. Ma, J. M. Luther, Joule **4**, 1160 (2020); https://doi.org/10.1016/j.joule.2020.04.006

[6] Q. Mahmood, M. Yaseen, M. Hassan, M.S. Rashid, I. Tlili, A. Laref, Mater. Res. Express. **6**, 045901 (2019); https://doi.org/10.1088/2053-1591/aaf997

[7] M. M. Saad H.-E., B. O. Alsobhi, ACS Omega **7**(32), 27903 (2022); https://doi.org/10.1021/acsomega.2c01511

[8] A. M. Shawahni, M. S. Abu-Jafar, R. T. Jaradat, T. Ouahrani, R. Khenata, A. A. Mousa, K. F. Ilaiwi, Materials **11**, 2057 (2018); https://doi.org/10.3390/ma11102057

[9] L. Protesescu, S. Yakunin, M. I. Bodnarchuk, F. Krieg, R. Caputo, C. H. Hendon, R. X. Yang, A. Walsh, M. V. Kovalenko, Nano Lett. **15**, 3692 (2015); https://doi.org/10.1021/nl5048779

[10] S. Gupta, T. Bendikov, G. Hodes, D. Cahen, ACS Energy Lett. **1**(5), 1028 (2016); https://doi.org/10.1021/acsenergylett.6b00402

[11] A. Almeshal, M. M. Saad H.-E., B. O. Alsobhi, J. Ovonic Res. **19**(1), 113 (2023); https://doi.org/10.15251/JOR.2023.191.113

[12] M. A. Ali, R. Ullah, S. A. Dar, G. Murtaza, A. Khan, A. Mahmood, Phys. Scr. **95**, 075705 (2020); https://doi.org/10.1088/1402-4896/ab8eee

[13] M. R. U. Hashmi, M. Zafar, M. Shakil, A. Sattar, S. Ahmed, S. A. Ahmad, Chinese Phys. B **25**, 117401 (2016); https://doi.org/10.1088/1674-1056/25/11/117401

[14] N. Hasan, M. Arifuzzaman, A. Kabir, RSC Adv. **12**, 7961 (2022); https://doi.org/10.1039/d2ra00546h

[15] M. Houari, B. Bouadjemi, M. Matougui, S. Haid, T. Lantri, Z. Aziz, S. Bentata, B. Bouhafs, Opt. Quant. Electron. **51**, 234 (2019); https://doi.org/10.1007/s11082-019-1949-y

[16] L. Ali, M. Ahmad, M. Shafiq, T. Zeb, R. Ahmad, M. Maqbool, I. Ahmad, S. J. Asadabadi, B. Amin, Mater. Today Commun. **25**, 101517 (2020); https://doi.org/10.1016/j.mtcomm.2020.101517

[17] S. Yalameha, P. Saeid, Z. Nourbakhsh, A. Vaez, A. Ramazani, Appl. Phys. **127**, 085102 (2020); https://doi.org/10.1063/1.5125920

[18] K. Khan, J. Sahariya, A. Soni, Mater. Chem. Phys. **262**, 12428 (2021); https://doi.org/10.1016/j.matchemphys.2021.124284

[19] M. A. Islam, M. Z. Rahaman, S. K. Sen, AIP Adv. **11**, 075109 (2021); https://doi.org/10.1063/5.0057287

[20] M. M. Saad H-.E. S. E. A. Yousif, Chalcogenide Lett. **19**, 153 (2022); https://doi.org/10.15251/cl.2022.192.153

[21] K. A. Parrey, T. Farooq, S. A. Khandy, U. Farooq, A. Gupta, Comput. Condens. Matter **19**, e00381 (2019; https://doi.org/10.1016/j.cocom.2019.e00381

[22] M. S. Hossain, M. M. H. Babu,T. Saha, M. S. Hossain, J. Podder, M. S. Rana, A. Barik, P. Rani, AIP Adv. **11,** 055024 (2021); https://doi.org/10.1063/5.0048979

[23] D. Saikia, M. Alam, J. Bera, A. Betal, A. N. Gandi, S. Sahu, Adv. Theory Simul. **5**(12), 2200511 (2022); https://doi.org/10.1002/adts.202200511

[24] H. Joshi, R. K. Thapa, A. Laref, W. Sukkabot, L. Pachuau, L. Vanchhawng, P. G. Gallardo, M. M. Saad H.-E., D.P. Rai, Surf. Interfaces **30**, 101829 (2022); https://doi.org/10.1016/j.surfin.2022.101829

[25] P. Hohenberg, W. Kohn, Phys. Rev. B **136**, 864 (1964); https://doi.org/10.1103/PhysRev.136.B864

[26] K. H. Schwarz, P. Blaha, G. K. H. Madsen, Comput. Phys. Commun. **147**, 71 (2002); https://doi.org/10.1016/S0010-4655(02)00206-0

[27] J. P. Perdew, K. Burke, M. Ernzerhof, Phys. Rev. Lett. **77**, 3865 (1996); https://doi.org/10.1103/PhysRevLett.77.3865

[28] W. Kohn, L. J. Sham, Phys. Rev. **140** A, 1133 (1965); https://doi.org/10.1103/PhysRev.140.A1133

[29] F. D. Murnaghan, PNAS **30**(9), 244 (1944). https://doi.org/10.1073/pnas.30.9.244

[30] M. H. Rahman, M. Jubair, M. Z. Rahaman, M. S. Ahasan, K. Ostrikov, M. Roknuzzaman, RSC Adv. 1**2**, 7497 (2022); https://doi.org/10.1039/D2RA00414C

[31] U. G. Jong, C. J. Yu, Y. H. Kye, Y. G. Choe, W. Hao, S. Li, Inorg. Chem. **58**, 4134 (2019); https://doi.org/10.1021/acs.inorgchem.8b03095

[32] L.-C. Tang, Y.-C. Chang, J.-Y. Huang, M.-H. Lee, C.-S. Chang, Jap. J. Appl. Phys. **48**, 112402 (2009); https://doi.org/10.1143/JJAP.48.112402

[33] M. Roknuzzaman, K. Ostrikov, H. Wang , A. Du, T. Tesfamichael, Sci. Rep. **7**, 14025 (2017); https://doi.org/10.1038/s41598-017-13172-y

[34] S. Chen, T. Bimenyimana, M. Guli, Results Phys. **14**, 102408 (2019); https://doi.org/10.1016/j.rinp.2019.102408

[35] W. Travis, E. N. K. Glover, H. Bronstein, D. O. Scanlon, R. G. Palgrave, Chem. Sci. **7**, 4548 (2016); https://doi.org/10.1039/c5sc04845a

[36] R. D. Shannon, Acta Cryst. A **32**, 751 (1976); https://doi.org/10.1107/S0567739476001551

[37] V. M. Goldschmidt, D. Naturwiss. **14**, 477 (1926); https://doi.org/10.1007/BF01507527

[38] S. Korbel, M. A. L. Marques, S. Botti, J. Mater. Chem. C **4**, 3157 (2016); https://doi.org/10.1039/C5TC04172D

[39] M. Houari, B. Bouadjemi, S. Haid, M. Matougui, T. Lantri, Z. Aziz, S. Bentata, B. Bouhafs, Indian J. Phys. **94**, 455 (2020);

[40] M. S. Alam, M. Saiduzzaman, A. Biswas, T. Ahmed, A. Sultana, K. M. Hossain, Sci. Rep. **12**, 8663 (2022); https://doi.org/10.1038/s41598-022-12713-4

[41] D. B. Raja, R. Vidya, K. S. Sundaram, Solar Energy **245**, 353 (2022); https://doi.org/10.1016/j.solener.2022.09.024

[42] K. Wang, G. Li, S. Wang, S. Liu, W. Sun, C. Huang, Y. Wang, O. Song, S. Xiao, Adv. Mater. **30**, 1801481 (2018); https://doi.org/10.1002/adma.201801481